Available online at www.sciencedirect.com

SciVerse ScienceDirect

Ceramics International 39 (2013) 415–423

CERAMICS INTERNATIONAL

www.elsevier.com/locate/ceramint

Significant improvement in the electrochemical performances of nano-nest like amorphous MnO_2 electrodes due to Fe doping

D.P. Dubal[a,b], C.D. Lokhande[b,*]

[a]*Technische Universität Chemnitz, Institut für Chemie, AG Elektrochemie, D-09107 Chemnitz, Germany*
[b]*Thin Film Physics Laboratory, Department of Physics, Shivaji University, Kolhapur 416004 (M.S), India*

Received 10 June 2012; received in revised form 14 June 2012; accepted 14 June 2012
Available online 23 June 2012

Abstract

Amorphous and highly porous nanonest like Fe:MnO_2 thin films have been potentiostatically synthesized and are characterized by using X-ray diffraction (XRD), Field emission scanning electron microscopy (FESEM), Energy dispersive X-ray analysis (EDAX), Fourier transform infrared spectroscopy (FTIR), wettability test and optical properties. The supercapacitive performance of Fe:MnO_2 electrodes were tested using cyclic voltammetry (CV), charge–discharge and impedance techniques in 1 M Na_2SO_4 electrolyte. The effect of Fe doping on structural, morphological, compositional and supercapacitive properties of MnO_2 thin films has been investigated. Further, the effect of electrolyte concentration and scan rate on the supercapacitance of MnO_2 and Fe:MnO_2 electrodes have been studied. The results showed that as Fe doping concentration increases up to 2 at% the supercapacitance increases from 166 to 231 F g^{-1}. The maximum specific capacitance of 273 F g^{-1} was achieved for 2 at% Fe:MnO_2 at 5 mV s^{-1} scan rate.

Keywords: Amorphous MnO_2; Impedance; Nano-nest; Supercapacitor

1. Introduction

Owing to the exceedingly rich structural variety and chemistry that they display, as well as their low cost and environmental friendliness, manganese oxides find extensive applications in electrochemical energy storage and conversion. They are used in commercial Zn/MnO_2 alkaline cells and zinc/air cells, and have been extensively investigated as intercalation cathodes for rechargeable lithium batteries [1]. More recently, there have been reports on manganese oxides as electrodes for electrochemical supercapacitors [2–4]. While investigations have focused most extensively on numerous crystalline structures of manganese oxides, increasing attention has been given to non-crystalline, including amorphous and nanocrystalline compounds. Amorphous or nanocrystalline manganese oxides reported earlier [5,6] exhibit much higher lithium intercalation capacity than their crystalline counterparts and in some cases also excellent cycling performance. Recently, amorphous and nanocrystalline manganese oxides have also been shown to be promising electrode materials for electrochemical supercapacitors [7,8].

The preparation methods of Mn oxides for supercapacitor applications include thermal decomposition [9], co-precipitation [10], sol–gel processes [2], physical vapor deposition [11], hydrothermal synthesis [12], and anodic deposition [8]. Recent research is focused on increasing the specific capacitance of the oxides by introducing other oxides technology [13]. The capacitance of MnO_2 electrode is believed to be predominant due to pseudocapacitance, which is attributed to reversible redox transitions involving exchange of protons and/or cations with the electrolyte [14]. However, the resistivity and the equivalent series resistance (ESR) of MnO_2 electrode are very large. Therefore, its capacity is limited. In order to overcome this disadvantage, the composite electrode materials of the manganese oxide were prepared with a conducting additive such as carbon material (graphite, carbon nanotube, porous carbon, activated carbon, and carbon aerogel, etc.) [15], conducting polymers [16], metal oxides [17,18] etc.

In order to improve the pseudocapacitive properties of plain Mn oxide, the addition of other transition metal

*Corresponding author. Tel.: +91 231 2609225; fax: +91 231 2692333.
E-mail address: l_chandrakant@yahoo.com (C.D. Lokhande).

0272-8842/$36.00
http://dx.doi.org/10.1016/j.ceramint.2012.06.042

oxides has been attempted. Studies have found that the incorporation of Ni [2,11–13], Co [18,17], V [19] and Mo [20] oxides could enhance the specific capacitances of Mn-based oxides. Recently, crystalline $MnFe_2O_4$ with a spinel structure, which could exhibit pseudocapacitive behavior, was found to have wonderful cyclic stability. However, its specific capacitance was only around 100 F g^{-1} [13]. In contrast, Lee et al. [21] indicated that hydrous Mn–Fe mixed oxide, in which the Mn oxide was nanocrystalline and the Fe oxide seemed to be amorphous in nature, can be prepared by anodic deposition. An optimum specific capacitance of the binary oxide was over 200 F g^{-1}.

In present investigation, nano-nest like amorphous Fe:MnO_2 thin films are successfully synthesized by potentiostatic deposition and used as potential candidate for supercapacitor. The effect of Fe doping on structural, morphological, compositional, wettability and supercapacitive properties of MnO_2 thin films have been investigated. The effect of electrolyte concentration and scan rate on specific capacitance of MnO_2 and Fe:MnO_2 electrodes have been studied. Also stability, charge–discharge and impedance of MnO_2 and Fe:MnO_2 electrodes have been studied.

2. Experimental

The MnO_2 and Fe:MnO_2 thin films were electrodeposited at room temperature from aqueous alkaline bath. The bath consisted of 0.1 M manganese sulphate ($MnSO_4 \cdot 4H_2O$) complexed with 0.1 M citric acid {C (OH) (COOH) $(CH_2COOH)_2 \cdot H_2O$} maintained at a pH of ~10.5 through the addition of 1 M sodium hydroxide (NaOH) solution. In order to dope Fe in MnO_2 thin films, four different concentrations (0.5, 1, 2 and 4 at%) were selected. The solution was prepared in freshly prepared double distilled water. Mirror polished and ultrasonically cleaned stainless steel was used as substrates.

In electrodeposition, the graphite substrate (4 cm × 1.5 cm) was used as the anode. A saturated calomel electrode (SCE) was used as the reference electrode in conventional three electrode system. An EG & G Princeton Applied Research (model 263-A) potentiostat was employed for deposition. The anodic deposition of MnO_2 and Fe:MnO_2 film was performed at 1.1 V/SCE potential. After electrodeposition, the electrode was dried in air. Grayish black colored, smooth, uniform and well adherent MnO_2 and Fe:MnO_2 thin films were obtained by the potentiostatic method.

Crystal structures of MnO_2 and Fe:MnO_2 electrodes were analyzed by X-ray diffraction within the range 10°–100° on computer controlled Philips PW-3710 using CrK_α radiations ($\lambda = 2.2897$ Å). The surface morphologies and compositional studies of electrodes were carried out by FE-SEM (field emission scanning electron microscopy, Model: JSM-6701F, JEOL, Japan) attached with an energy-dispersive X-ray analysis (EDAX) analyzer to measure the sample composition. The Fourier transform infrared (FTIR) spectra of the samples were collected using a 'Perkin Elmer, FTIR Spectrum one' unit. In order to study interaction between electrolyte and electrode surface contact angle measurement was carried out by Rame-hart USA equipment with CCD camera. Electrochemical performance of the deposited oxides was evaluated using cyclic voltammetry (CV) in 1 M Na_2SO_4 electrolyte. The test was performed in a three-electrode cell, in which the oxide electrode was assembled as the working electrode. In addition, a platinum sheet and a SCE were used as the counter electrode and the reference electrode, respectively. The measuring instrument was a 263 A EG & G Princeton Applied Research Potentiostat. The galvanostatic charge–discharge measurement was carried out with 8-channel advanced battery cycler (WonA-Tech-WBCS-3000 model). Electrochemical impedance spectroscopy (EIS) measurements were recorded using the multi-impedance test system after the first cycle. The frequency range was from 10 kHz to 10 mHz with an AC amplitude of 10 mV

3. Results and discussion

3.1. Potentiostatic deposition of MnO_2 and Fe:MnO_2

Fig. 1 shows potentiostatic curves during the formation of MnO_2 and Fe:MnO_2 recorded on stainless steel (SS) substrate with applied potential of 1.1 V/SCE. At the initial stage of electrodeposition, drastic increase in current density was noted, indicating the formation of Helmholtz layer of $Mn(OH)_2^+$ ions at the interface between SS substrate and electrolyte. Moreover, the initiation of electron transfer process corresponding to nucleation process of MnO_2 on stainless steel shows the stage where current density was immensely reduced. Therefore, in presence of Fe, the current density of nucleation part was lower and the current density versus time variation was much steeper. In addition, the steady flow of current density after nucleation process, implying uniform growth

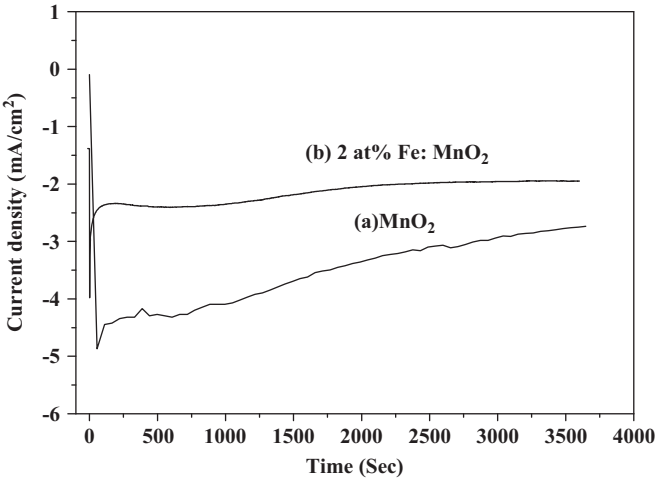

Fig. 1. Potentiostatic curves of MnO_2 and 2 at% Fe:MnO_2 thin films in aqueous alkaline bath at 1.1 V/SCE.

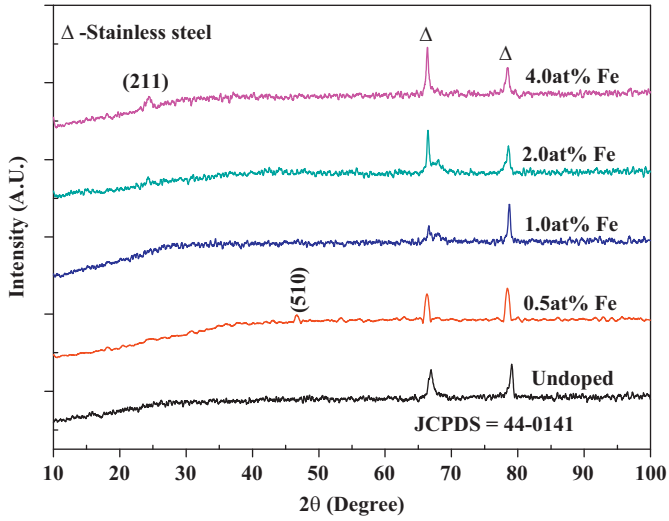

Fig. 2. XRD patterns of MnO_2 and Fe:MnO_2 thin films prepared with respect to different Fe concentrations onto stainless steel substrate.

of MnO_2 crystallite. This growth process was slightly slow in the Fe:MnO_2.

$$2Mn(OH)_2^+ + 2e^- \Rightarrow 2MnOOH + H_2\uparrow \quad (1)$$

$$2MnOOH + 2e^- \Rightarrow 2MnO_2 + H_2\uparrow \quad (2)$$

Therefore, this indicates that the nucleation and film growth processes can be altered in presence of Fe [21]. The higher potential and alkaline medium assist the formation of MnO_2.

3.2. Structural studies

Fig. 2 shows the XRD patterns of MnO_2 and Fe:MnO_2 thin films grown on stainless steel substrates with different Fe concentrations ranging from 0.5 to 4 at%. There are very tiny peaks are observed in 0.5 and 4 at% Fe doping, corresponding to (510) and (211) planes, respectively. These

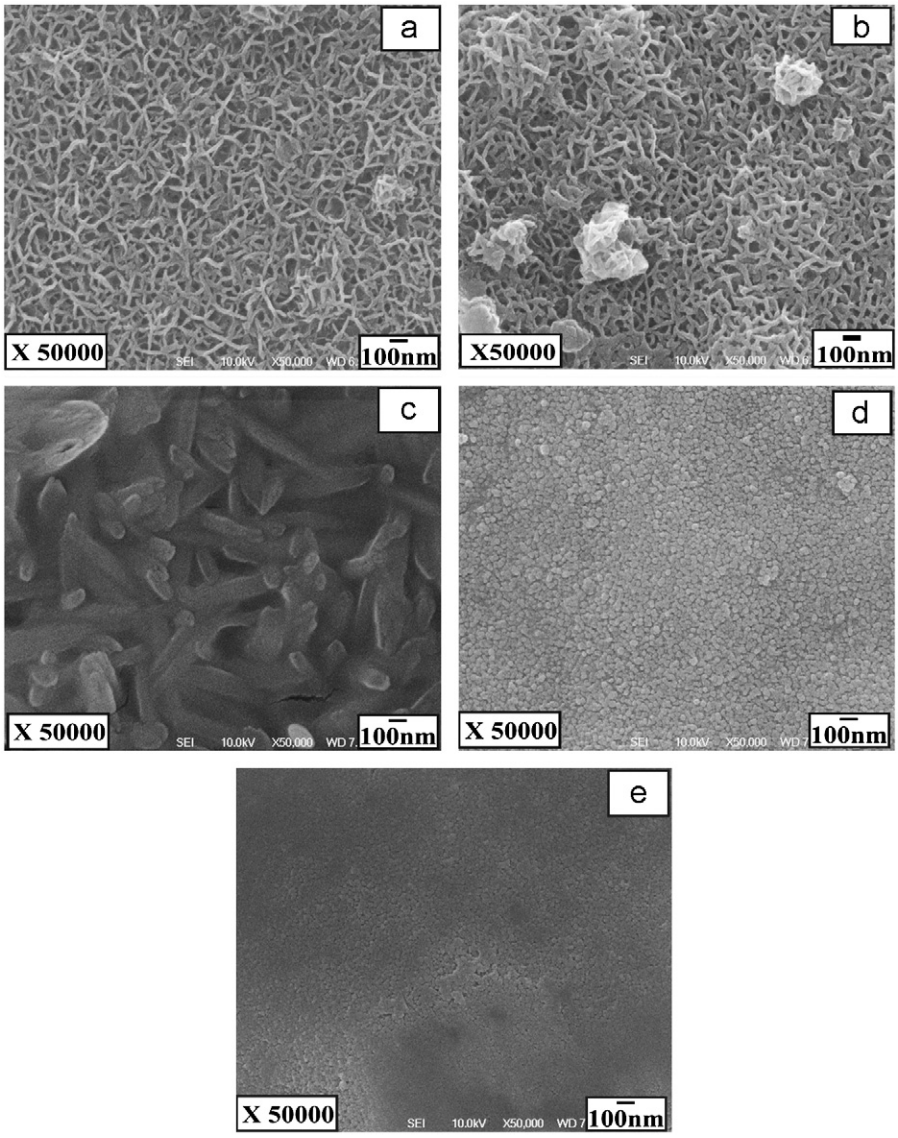

Fig. 3. SEM images of (a) MnO_2 (b) 0.5 at% Fe (c) 1 at% Fe (d) 2 at% Fe (e) 4 at% Fe:MnO_2 thin films at $\times$ 50,000 magnification.

two planes are associated with MnO_2 [JCPDS=44-0141] and remaining all the peaks observed in the XRD patterns are due to stainless steel substrate and are indexed by the triangles. The observed peak intensity is too low which confirms that the incorporated Fe oxide could be amorphous and did not change the amorphous nature of deposited manganese oxide. Similar type of behavior has been reported by Lee et al. [21] for Fe doped MnO_2 thin films on graphite substrate. In supercapacitor applications, amorphous phase is preferred due to easy penetration of ions through the bulk of the active material [22].

3.3. Surface morphological and EDAX studies

Nucleation and growth processes are considered as the important factors in surface morphology alteration. The surface morphology of MnO_2 can be altered by changing nucleation and growth stages of MnO_2. Fig. 3(a–e) illustrates the effect of presence of Fe on the surface morphology of MnO_2 electrode. The surface of the MnO_2 sample (Fig. 3a) is made up of 3D network of nano-nests like architecture. The approximate width of this nano-nest is about 10–20 nm. For 0.5 at% Fe doping (Fig. 3b) there is no any significant difference has been observed (may be due to less Fe doping concentration). Further as Fe doping concentration increases to 1 at% (Fig. 3c), this nano-nests like morphology gets converted into randomly oriented nanorods. In this case surface of MnO_2 becomes slightly rough. As the Fe concentration in the plating solution continuously raised to 2.0 at%, nanorods converts into highly porous and rougher deposited oxide (Fig. 3d). Due to Fe addition, the surface of the MnO_2 electrode becomes rough. However, as can be confirmed in Fig. 3e, the surface roughness began to decrease as the Fe addition in the plating solution was further increased. The surface became flat and was even smoother than the plain MnO_2. Thus, result indicates that up to 2 at% the Fe addition modifies the surface of the MnO_2 electrode. Note that shifting from MnO_2 to Fe:MnO_2 materials lead to a drastic increase in the surface area. This type of highly amorphous and highly porous structures is expected to produce high supercapacitance values.

To study size, shape and orientation of crystallites, TEM, SAED and HRTEM images were studied. Fig. 4(a–c) shows transmission electron micrograph, corresponding SAED pattern and high resolution transmission electron micrograph of MnO_2 film respectively. Fig. 4(a) shows that the growth has taken place 'cluster by cluster' and randomly oriented nanocrystals are formed so that it looks like a rod along with amorphous matrix. The crystallites are grown together to form clusters where the crystallites are indistinguishable. Fig. 4(b) shows corresponding selected area electron diffraction (SAED) pattern of MnO_2 nano-nest. The blurred bright electron diffraction rings show that the MnO_2 film is amorphous or poorly crystalline, supporting to X-ray diffraction results. The high resolution transmission electron micrograph of individual nano-nest indicates that the MnO_2 nanonests produced here have amorphous nature.

Fig. 5(a and b) shows typical EDAX patterns for MnO_2 and Fe:MnO_2 thin films on ITO substrate. The elemental analysis was carried out for Mn and Fe. Here some unexpected but physically present elements like Si and Sn were detected due to glass substrate and ITO coated conduction layer, respectively. The strong peaks for Mn

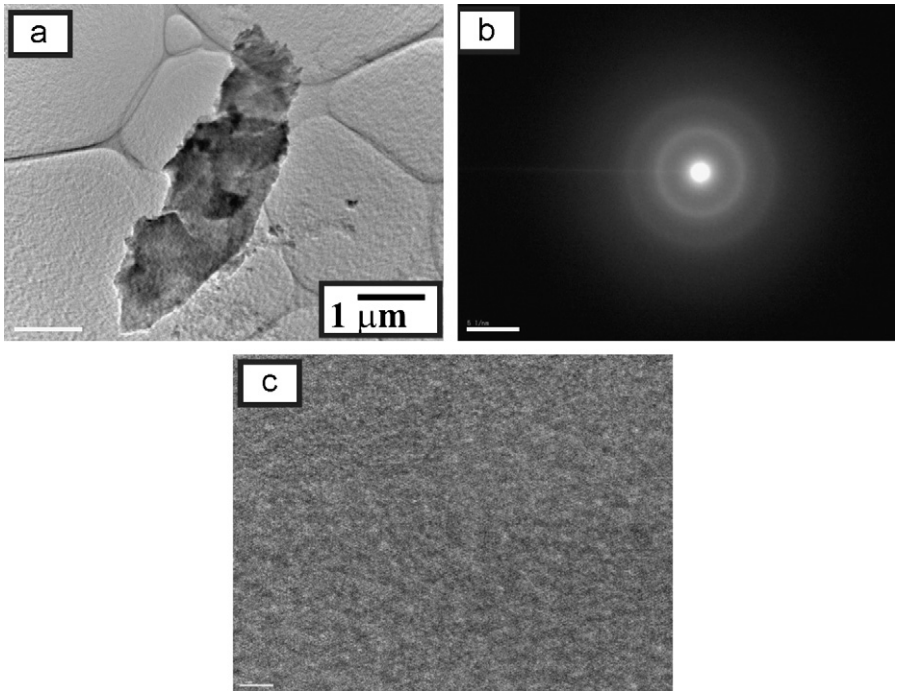

Fig. 4. (a) TEM (b) SAED (c) HRTEM images of MnO_2 thin film.

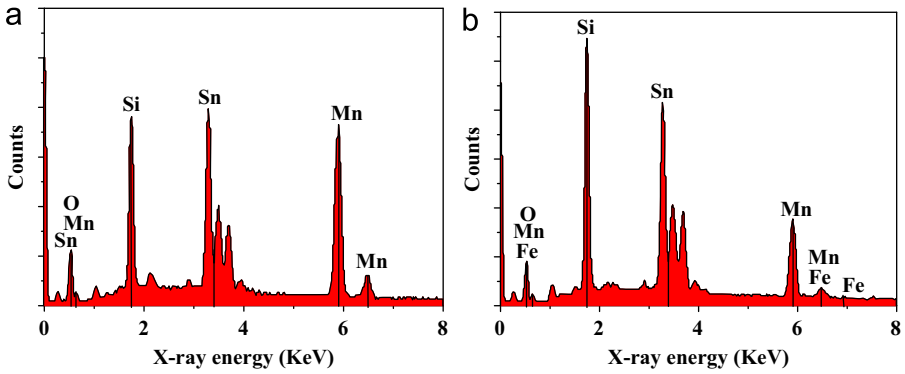

Fig. 5. EDAX spectra of (a) MnO_2 and (b) 2 at% Fe:MnO_2.

Table 1
Elemental composition of manganese and iron in atomic %.

Elements	Mn-K	Fe-K
MnO_2	50.00	0
2 at% Fe:MnO_2	48.73	1.02

and O were found in both the spectra (Fig. 5(a and b)), and in Fig. 5(b) there are small elemental peaks which are due to Fe. Thus the existence of Fe was confirmed from the EDAX spectrum. The average atomic percentage of Mn:Fe was listed in the Table 1. Thus from elemental analyses, it is confirmed that, for 2 at% Fe in plating bath only 1.02 at% Fe has resulted into MnO_2 sample.

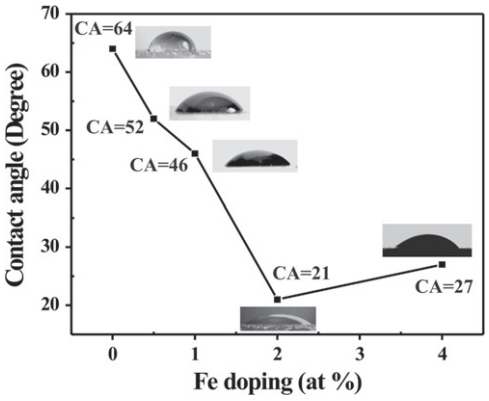

Fig. 6. Contact angles for MnO_2 and Fe:MnO_2 (0.5, 1, 2 and 4 at%) thin films.

3.4. Surface wettability test

Wettability involves the interaction between a liquid and a solid in contact. The wetting behavior is characterized by the value of the contact angle, a microscopic parameter. If the wettability is high, contact angle (θ), will be small and the surface is hydrophilic. On the contrary, if the wettability is low, θ will be large and the surface is hydrophobic. The contact angle is an important parameter in surface science and its measurement provides a simple and reliable technique for the interpretation of surface energies. Fig. 6 shows the systematic presentation of measurement of contact angles for MnO_2 and Fe:MnO_2 thin films. The nano-nest like MnO_2 thin film showed a contact angle of about 64°. Here the water contact is slightly high this may be due to the air trapped inside nano-nest network which prevents the water for adhering to the film. As the Fe doping concentration increases up to 2 at% the water contact angles of MnO_2 thin films decreases due to increased surface energy. Generally high surface energy exhibits low water contact angle [23]. The contact angles were found to be 52°, 46° and 21° for 0.5, 1.0 and 2.0 at%, respectively as seen from Fig. 6. This indicates that with increasing Fe doping concentration, the contact angle decreases and finally film surface becomes more hydrophilic. This is useful for making the intimate contact of electrolyte with MnO_2 thin film (electrode). Hydrophilicity is attributed to amorphous nature. Amorphous material with hydrophilic nature is one of the key requirements for supercapacitor electrode material. Further increase in Fe doping concentration decreases the porosity of the MnO_2 electrode and hence there is again increase in the contact angle.

3.5. FTIR studies

FTIR spectroscopy analysis can be an alternative to X-ray being sensitive also to amorphous components and to the structural environment of the hydrous components, which can be diagnostic for a specific mineral phase of MnO_2 [24]. The region below 1400 cm^{-1} contains peaks due to fundamental vibrations of octahedral MnO_6 and the region above 1400 cm^{-1} contains peaks primarily corresponding to OH vibrations [25]. The regions from 750–600 cm^{-1} and 600–450 cm^{-1} correspond to Mn–O stretching and bending vibrations. Fig. 7(a and b) shows the FTIR spectra of MnO_2 and Fe:MnO_2 (2 at%) samples, respectively. In both the spectra, there is broad and intense peak at 3340 cm^{-1} related to –OH stretching vibrations. The absorption peaks around 1627 and 1110 cm^{-1} may be attributed to –OH bending vibrations combined with Mn

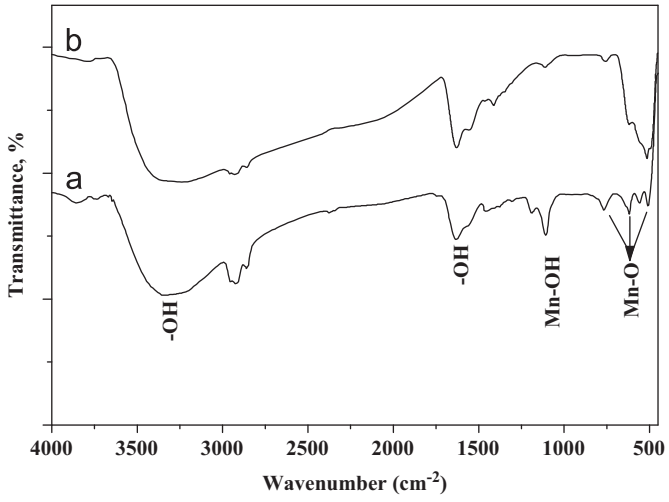

Fig. 7. FTIR spectra of (a) MnO_2 and (b) Fe:MnO_2 samples.

atoms [26]. The absorption of the Mn–O lattice vibrations around at 765, 620 and 512 cm^{-1} in the spectrum is indicative of a tetragonally distorted cubic lattice. These absorption peaks may be associated with the coupling mode between Mn–O stretching modes of tetrahedral and octahedral sites [27,26]. These for MnO_2 associated with the coupling mode between Mn–O stretching modes of tetrahedral and octahedral sites shifted slightly towards lower wavenumbers after Fe doping. The IR result suggests the presence of somewhat bound water in the MnO_2 and Fe:MnO_2 structure, which is generally believed to be favorable to the electrochemical activity of the material.

3.6. Supercapacitive properties

Cyclic voltammetry (CV) is considered to be an ideal tool to indicate the capacitive behavior of any material. A large magnitude of current and a rectangular type of voltammogram, symmetric in anodic and cathodic directions, are the indications of ideal capacitive nature of any material.

3.6.1. Effect of Fe doping concentration

Electrochemical behavior of the deposited oxides was evaluated using CV in 1 M Na_2SO_4 electrolyte with a potential scan rate of 100 mV s^{-1}. The slightly rectangular shapes and mirror-image characteristics of the CV curves reveal the ideal pseudocapacitive behavior of all the electrodes, indicating that the deposited binary Fe:MnO_2 are promising electrode materials for use in supercapacitors. The values of supercapacitance calculated from the CVs are 166, 192, 216, 231 and 208 F g^{-1} for undoped, 0.5, 1.0, 2.0 and 4 at% Fe, respectively. It is clear from Fig. 8 that as Fe doping concentration increases up to 2 at%, the supercapacitance of MnO_2 electrode increases from 166 to 231 F g^{-1}. Further increase in Fe doping concentration (4 at%) decreases the supercapacitance. This may be due to the decrease in the porosity of the MnO_2 electrode which reduces the surface area of electrode. In Fig. 8, although the shapes of CV curves are similar, 2 at% Fe:MnO_2 has the largest enclosed area, reflecting its superior charge-storage performance. The data indicates that the specific capacitance remarkably increases from 166 F g^{-1} for MnO_2 to 231 F g^{-1} for 2 at% Fe:MnO_2. However, further increasing the Fe content in the binary oxide causes the reverse effect; the specific capacitance of 4 at% Fe:MnO_2 is only 208 F g^{-1}. The experimental results, shown in Fig. 8, clearly show that the amount of Fe oxide added significantly affects the overall capacitance of the deposited binary Mn–Fe oxide. The value reported in this study is comparable with the values reported in the literature [28].

3.6.2. Effect of scan rate

The high or pulse-power property of 2 at% Fe:MnO_2 electrode is examined by using cyclic voltammetry at different scan rates. Typical CV curves measured at 5, 10, 20, 50, 75 and 100 mV s^{-1} in 1 M Na_2SO_4 electrolyte within voltage range of +0.9 to −0.1 V/SCE electrode are shown in Fig. 9 along with the current under the curve increases slowly with the scan rate. The specific capacitance values decreased from 273 to 231 F g^{-1} for Fe:MnO_2 electrode. Fig. 10 shows the variation of specific and interfacial capacitance of Fe:MnO_2 thin films with scan rate. The maximum specific capacitance obtained for Fe:MnO_2 was 273 F g^{-1}. The dependence of the voltammetric charge of Fe:MnO_2 in 1 M Na_2SO_4 solution on the scan rate can be understood by the slow diffusion of Na^+ ions into the pores of Fe:MnO_2 [10]. At high scan rates, diffusion limits the movement of Na^+ ions due to time constraint, and only the outer active surface is utilized for the charge storage. However, at lower scan rates, all the active surface area can be utilized for charge storage. Hence, the specific capacitance obtained at the slowest scan rate is believed to be closest to that of full utilization of the electrode material.

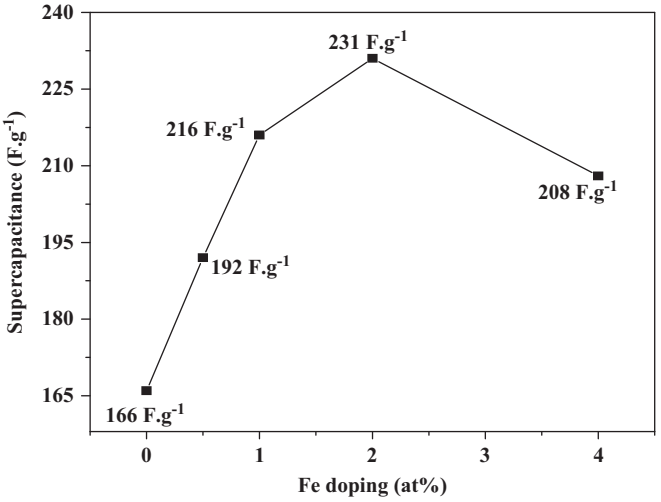

Fig. 8. Variation of supercapacitance with Fe doping concentration.

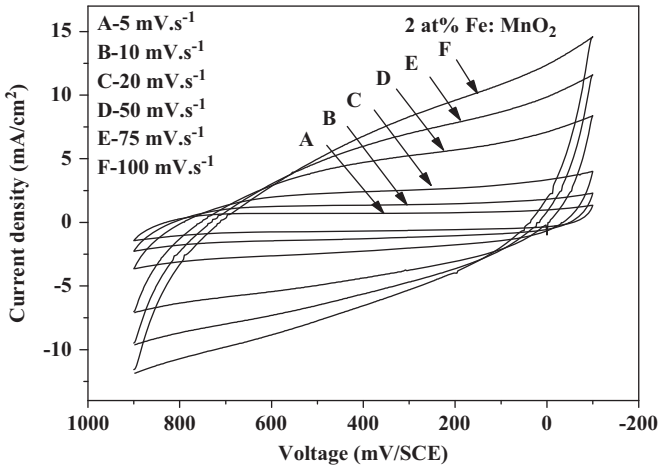

Fig. 9. Cyclic voltammograms of 2 at% Fe:MnO_2 electrode at different scanning rates in 1 M Na_2SO_4 electrolyte.

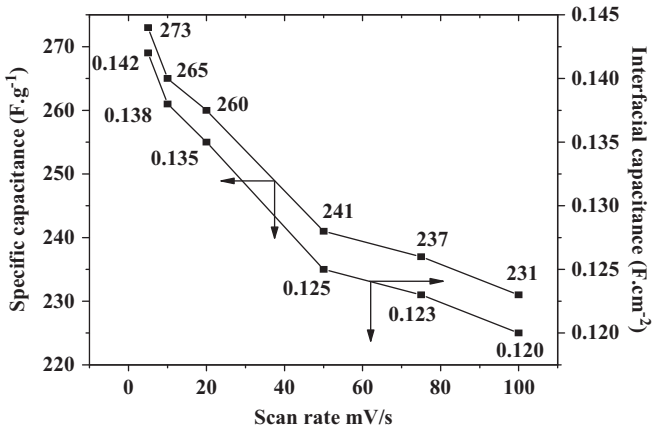

Fig. 10. Variation of specific and interfacial capacitance of 2 at% Fe:MnO_2 thin films with scan rate.

3.6.3. Stability studies

The electrochemical stability of the Fe:MnO_2 electrodes were evaluated by repeating the CV test for 1000 cycles at 100 mV s^{-1} scan rate. The variation of specific capacitance with cycle number for the electrodes is presented in Fig. 11 which shows that specific capacitance decreases with increasing the cycle number. The specific capacitance of both the electrodes remains almost constant up to 1000 cycles but thereafter declines slightly. The capacitance retained ratios after 1000 cycles (capacitance at the 1000th cycle/capacitance at the 1st cycle) of the MnO_2 and Fe:MnO_2 electrodes were 89% and 92%, respectively. This implies an excellent long-term recycling capability. Lee et al. [21] reported that the addition of Fe oxide effectively increased the capacitance retained ratio of MnO_2 after cycling.

3.6.4. Galvanostatic charge–discharge studies

The galvanostatic charge/discharge profile of the MnO_2 and Fe:MnO_2 electrodes in 1 M Na_2SO_4 electrolyte are

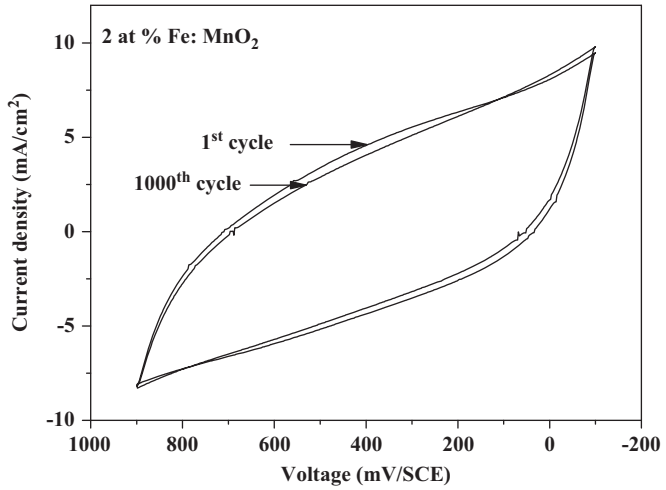

Fig. 11. Cyclic voltammograms of 2 at% Fe:MnO_2 electrode at different cycles at 100 mV s^{-1} scan rate.

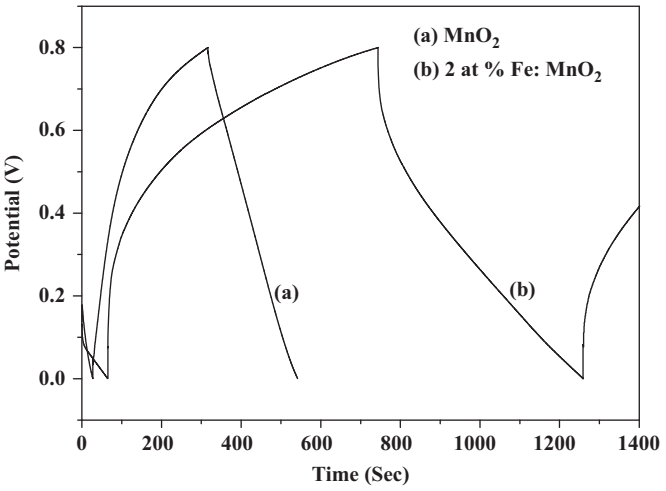

Fig. 12. Galvanostatic charge–discharge curves of (a) MnO_2 and (b) 2 at% Fe:MnO_2 electrodes in 1.0 M Na_2SO_4 electrolyte.

presented in Fig. 12. The charge/discharge current rate is 2 mA and the operational potential range is between 0 and 0.8 V/SCE. It can be seen that the charge profile is slightly curved, suggesting a pseudocapacitive characteristic. At the moment of electric current reversing from charging to discharging, a potential drop can be observed due to the electrode polarization at this high current rate. Except for the initial potential drop, the discharge profile is essentially linear.

For a specific power of 2.9 Wh/kg, the specific energy of the capacitor calculated to be 85.32 kW/kg for plain MnO_2 thin film. After 2 at% Fe doping the specific power slightly increases to 3.1 Wh/kg but increase in the specific energy was found i.e. 207.82 kW/kg. This large increase in specific energy may be due to increased time for charging and discharging of capacitor. Coulomb efficiency (η%) is less (72%) of Fe:MnO_2 than that for MnO_2, this may be due to slight greater iR drop observed in case of Fe:MnO_2. All the values of specific energy (SE), and specific power (SP) and

Table 2
Values of power density, energy density and coulomb efficiency of MnO_2 and 2 at% Fe:MnO_2 thin films.

Name	Specific energy (Wh/kg)	Specific power (W/kg)	Coulomb efficiency, η (%)
MnO_2	1.17	0.29×10^3	88.83
2 at% Fe:MnO_2	2.19	0.30×10^3	71.70

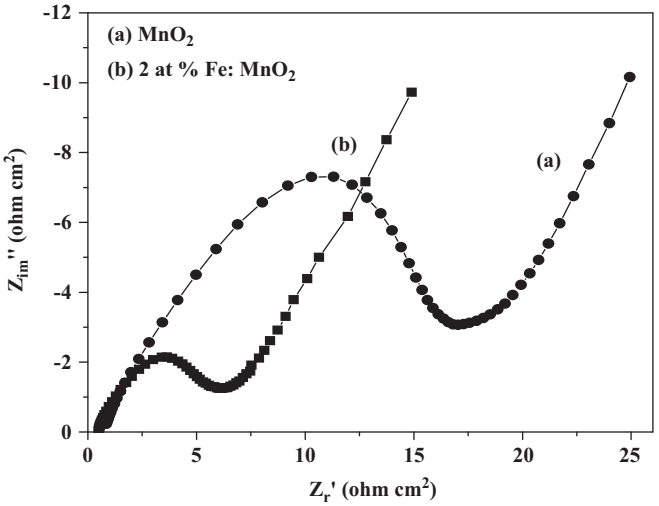

Fig. 13. Nyquist plots obtained for (a) MnO_2 and (b) 2 at% Fe:MnO_2 electrodes at 0.5 V over the frequency range 1 mHz–100 MHz.

coulomb efficiency (η %) for MnO_2 and Fe:MnO_2 are listed in Table 2.

3.6.5. Impedance analysis

Fig. 13 shows electrochemical impedance spectra in the form of Nyquist plots for MnO2 and Fe:MnO_2 electrodes at potentials 0.5 V/SCE, where Z' and Z'' are the real and imaginary parts of the impedance, respectively. As can be seen in Fig. 13, the plots obtained are composed of a semi-circle at high frequencies, which is related to Faradaic reactions. The linear curve at the low-frequency region can be attributed to the diffusion controlled process in the electrolyte. The initial non-zero intercept at Z' at the beginning of the semicircle is almost identical in both the curves and is due to the electrical resistance of electrolyte, which has the average value of 0.5 Ω in 1 M Na_2SO_4 electrolyte. The resistance projected by semi-circle is due to the active electrode material (R_e). Therefore, the resistance values of MnO_2 and Fe:MnO_2 are 17 and 7 Ω respectively. This implies that iron addition in MnO_2 lowers the charge transfer resistance and increases conductivity of MnO_2. Thus Fe:MnO_2 is most promising electrode material in supercapacitive technology.

4. Conclusions

Nano-nest like amorphous MnO_2 and Fe:MnO_2 thin films are successfully prepared by potentiostatic deposition. The Fe addition did not change the amorphous structure of the deposited MnO_2. The addition of Fe significantly alters the surface morphology and lead to a drastic increase in porosity which increases the pseudocapacitive performance of MnO_2. Fe doping is confirmed from EDAX patterns. Wettebility test shows that as Fe doping concentration increases the contact angle decrease which is useful in making intimate contact between electrode and electrolyte. The supercapacitance decreases with increase in scan rate. Maximum specific capacitance achieved for 2 at% Fe:MnO_2 was 273 F g^{-1}. Also the specific power and specific energy increased from 0.29 to 0.30 kW/kg and 1.17 to 2.19 Wh/kg respectively due to the Fe addition. Moreover, capacitance-retained ratio of the Fe:MnO_2 electrode after 1000 charge–discharge cycles was also improved from 89% to 92% due to Fe addition. Impedance analysis shows that Fe addition improves conductivity of MnO_2 by reducing the charge transfer resistance.

Acknowledgment

One of the authors Prof. C.D. Lokhande is grateful to All India Council for Technical Education (AICTE), New Delhi for financial support through the scheme F. no. 8023/BOR/RID/RPS-165/2009-10. Authors are also grateful to the Council for Scientific and Industrial Research (CSIR), New Delhi (INDIA) for financial support through the scheme no. 03(1165)/10/EMR-II.

References

[1] C.D. Lokhande, D.P. Dubal, O.S. Joo, Metal oxide thin film based supercapacitors, Current Applied Physics 11 (2011) 255.
[2] S.C. Pang, M.A. Anderson, T.W. Chapman, Novel electrode materials for thin-film ultracapacitors: comparison of electrochemical properties of sol–gel-derived and electrodeposited manganese dioxide, Journal of the Electrochemical Society 147 (2000) 444.
[3] D.P. Dubal, D.S. Dhawale, R.R. Salunkhe, C.D. Lokhande, Conversion of chemically prepared interlocked cubelike Mn_3O_4 to birnessite MnO_2 using electrochemical cycling, Journal of the Electrochemical Society 157 (2010) A812.
[4] X. Tang, Z.H. Liu, C. Zhang, Z. Yang, Z. Wang, Synthesis and capacitive property of hierarchical hollow manganese oxide nanospheres with large specific surface area, Journal of Power Sources 193 (2009) 939.
[5] J.J. Xu, G. Jain, J. Yang, Amorphous manganese oxides as lithium intercalation hosts prepared by oxidation of Mn(II) precursors, Electrochemical and Solid State Letters 5 (2002) A152.
[6] A.I. Palos, M. Anne, P. Strobel, Electrochemical lithium intercalation in disordered manganese oxides, Solid State Ionics 138 (2001) 203.
[7] H.Y. Lee, S.W. Kim, H.Y. Lee, Expansion of active site area and improvement of kinetic reversibility in electrochemical pseudocapacitor electrode, Electrochemical and Solid State Letters 4 (2001) A19.

[8] C.C. Hu, T.W. Tsou, Ideal capacitive behavior of hydrous manganese oxide prepared by anodic deposition, Electrochemistry Communications 4 (2002) 105.
[9] H.Y. Lee, V. Manivannan, J.B. Goodenough, Electrochemical capacitors with KCl electrolyte, Comptes Rendus de l'Académie des Sciences: Series IIC: Chemistry 2 (1999) 565.
[10] M. Toupin, T. Brousse, D. Belanger, Influence of microstucture on the charge storage properties of chemically synthesized manganese dioxide, Chemistry of Materials : A Publication of the American Chemical Society 14 (2002) 3946.
[11] B. Djurfors, J.N. Broughton, M.J. Brett, D.G. Ivey, Microstructural characterization of porous manganese thin films for electrochemical supercapacitor applications, Journal of Materials Science 38 (2003) 4817.
[12] V. Subramanian, H. Zhu, R. Vajtai, P.M. Ajayan, B. Wei, Hydrothermal synthesis and pseudocapacitance properties of MnO_2 nanostructures, The Journal of Physical Chemistry B 109 (2005) 20207.
[13] S.L. Kuo, J.F. Lee, N.L. Wu, Study on pseudocapacitance mechanism of aqueous $MnFe_2O_4$ supercapacitor, Journal of the Electrochemical Society 154 (2007) A34.
[14] S. Devaraj, N. Munichandraiah, High capacitance of electrodeposited MnO_2 by the effect of a surface-active agent, Electrochemical and Solid-State Letters 8 (2005) A373.
[15] S.B. Ma, K.W. Nam, W.S. Yoon, X.Q. Yang, K.Y. Ahn, K.H. Oh, K.B. Kim, Electrochemical properties of manganese oxide coated onto carbon nanotubes for energy-storage applications, Journal of Power Sources 178 (2008) 483.
[16] E.H. Liu, X.Y. Meng, R. Ding, J.C. Zhou, S.T. Tan, Potentiodynamical co-deposited manganese oxide/carbon composite for high capacitance electrochemical capacitors, Materials Letters 61 (2007) 3486.
[17] G.Y. Zhao, C.L. Xu, H.L. Li, Highly ordered cobalt-manganese oxide (CMO) nanowire array thin film on Ti/Si substrate as an electrode for electrochemical capacitor, Journal of Power Sources 163 (2007) 1132.
[18] D.P. Dubal, A.D. Jagadale, S.V. Patil, C.D. Lokhande, Simple route for the synthesis of supercapacitive Co–Ni mixed hydroxide thin films, Materials Research Bulletin 47 (2012) 1239.
[19] M. Nakayama, A. Tanaka, S. Konishi, K. Ogura, Effects of heat-treatment on the spectroscopic and electrochemical properties of a mixed manganese/vanadium oxide film prepared by electrodeposition, Journal of Materials Research 19 (2004) 1509.
[20] M. Nakayama, A. Tanaka, Y. Sato, T. Tonosaki, K. Ogura, Electrodeposition of manganese and molybdenum mixed oxide thin films and their charge storage properties, Langmuir : the ACS Journal of Surfaces and Colloids 21 (2005) 5907.
[21] M.T. Lee, J.K. Chang, W.T. Tsai, Effects of iron addition on material characteristics and pseudo-capacitive behavior of Mn-Oxide electrodes, Journal of the Electrochemical Society 154 (2007) A875.
[22] D.P. Dubal, D.S. Dhawale, R.R. Salunkhe, C.D. Lokhande, Effect of different modes of electrodeposition on supercapacitive properties of MnO_2 thin films, Applied Surface Science 257 (2011) 3378.
[23] D.S. Dhawale, D.P. Dubal, V.S. Jamadade, R.R. Salunkhe, C.D. Lokhande, Fuzzy nanofibrous network of polyaniline electrode for supercapacitor application, Synthetic Metals 160 (2010) 519.
[24] S.K. Apte, S.D. Naik, R.S. Sonawane, B.B. Kale, N. Pavaskar, A.B. Mandale, B.K. Das, Nanosize Mn_3O_4 (Hausmannite) by microwave irradiation method, Materials Research Bulletin 41 (2006) 647.
[25] M. Minakshi, P. Singh, T.B. Issa, S. Thurgate, R.D. Marco, Lithium insertion into manganese dioxide electrode in MnO_2/Zn aqueous battery Part II. Comparison of the behavior of EMD and battery grade MnO_2 in $Zn|MnO_2|$aqueous LiOH electrolyte, Journal of Power Sources 138 (2004) 319.
[26] M. Ocana, Uniform particles of manganese compounds obtained by forced hydrolysis of manganese(II) acetate, Colloid and Polymer Science 278 (2000) 443.
[27] C.M. Julien, M. Massot, C. Poinsignon, Lattice vibrations of manganese oxides Part I: Periodic structures, Spectrochimica Acta 60 (2004) 689.
[28] D.P. Dubal, W.B. Kim, C.D. Lokhande, Galvanostatically deposited Fe:MnO_2 electrodes for supercapacitor application, Journal of Physics and Chemistry of Solids 73 (2012) 18.